밀집성 쌍성의 형성과 진화

배영복 (CAU)

2024년 1월 31일

2024 수치상대론 및 중력파 겨울학교

Binary Compact Stars
as Sources of Gravitational-waves

Observation of Gravitational Waves (GWs)

- GWTC-1 (Gravitational-Wave Transient Catalog)
  - O1 (Sep. 12, 2015 - Jan. 19, 2016)
    - First detection of GWs
  - O2 (Nov. 30, 2016 - Aug. 25, 2017)
    - First detection of a binary neutron star inspiral
  - 11 GW sources
- GWTC-2, GWTC-2.1
  - O3a (Apr. 01, 2019 - Oct. 01, 2019)
  - 44 GW sources
- GWTC-3
  - O3b (Nov. 01, 2019 - Mar. 27, 2020)
  - 35 GW sources
- GWTC-4 ?
  - O4 (May, 24, 2023 -)
  - Hundreds of GW sources?

Event	M ($M_\odot$)	$\mathcal{M}$ ($M_\odot$)	m_1 ($M_\odot$)	m_2 ($M_\odot$)	χ_{eff}	D_{L} (Gpc)	z	M_{f} ($M_\odot$)	χ_{f}	$\Delta\Omega$ (deg^2)	SNR
GW191103_012549	$20.0^{+3.7}_{-1.8}$	$8.34^{+0.66}_{-0.57}$	$11.8^{+6.2}_{-2.2}$	$7.9^{+1.7}_{-2.4}$	$0.21^{+0.16}_{-0.10}$	$0.99^{+0.50}_{-0.47}$	$0.20^{+0.09}_{-0.09}$	$19.0^{+3.8}_{-1.7}$	$0.75^{+0.06}_{-0.05}$	2500	$8.9^{+0.3}_{-0.5}$
GW191105_143521	$18.5^{+2.1}_{-1.3}$	$7.82^{+0.61}_{-0.45}$	$10.7^{+3.7}_{-1.6}$	$7.7^{+1.4}_{-1.9}$	$-0.02^{+0.13}_{-0.09}$	$1.15^{+0.43}_{-0.48}$	$0.23^{+0.07}_{-0.09}$	$17.6^{+2.1}_{-1.2}$	$0.67^{+0.04}_{-0.05}$	640	$9.7^{+0.3}_{-0.5}$
GW191109_010717	112^{+20}_{-16}	$47.5^{+9.6}_{-7.5}$	65^{+11}_{-11}	47^{+15}_{-13}	$-0.29^{+0.42}_{-0.31}$	$1.29^{+1.13}_{-0.65}$	$0.25^{+0.18}_{-0.12}$	107^{+18}_{-15}	$0.61^{+0.18}_{-0.19}$	1600	$17.3^{+0.5}_{-0.5}$
GW191113_071753	$34.5^{+10.5}_{-9.8}$	$10.7^{+1.1}_{-1.0}$	29^{+12}_{-14}	$5.9^{+4.4}_{-1.3}$	$0.00^{+0.37}_{-0.29}$	$1.37^{+1.15}_{-0.62}$	$0.26^{+0.18}_{-0.11}$	34^{+11}_{-10}	$0.45^{+0.33}_{-0.11}$	3600	$7.9^{+0.5}_{-1.1}$
GW191126_115259	$20.7^{+3.4}_{-2.0}$	$8.65^{+0.95}_{-0.71}$	$12.1^{+5.5}_{-2.2}$	$8.3^{+1.9}_{-2.4}$	$0.21^{+0.15}_{-0.11}$	$1.62^{+0.74}_{-0.74}$	$0.30^{+0.12}_{-0.13}$	$19.6^{+3.5}_{-2.0}$	$0.75^{+0.06}_{-0.05}$	1400	$8.3^{+0.2}_{-0.5}$
GW191127_050227	80^{+39}_{-22}	$29.9^{+11.7}_{-9.1}$	53^{+47}_{-20}	24^{+17}_{-14}	$0.18^{+0.34}_{-0.36}$	$3.4^{+3.1}_{-1.9}$	$0.57^{+0.40}_{-0.29}$	76^{+39}_{-21}	$0.75^{+0.13}_{-0.29}$	980	$9.2^{+0.7}_{-0.6}$
GW191129_134029	$17.5^{+2.4}_{-1.2}$	$7.31^{+0.43}_{-0.28}$	$10.7^{+4.1}_{-2.1}$	$6.7^{+1.5}_{-1.7}$	$0.06^{+0.16}_{-0.08}$	$0.79^{+0.26}_{-0.33}$	$0.16^{+0.05}_{-0.06}$	$16.8^{+2.5}_{-1.2}$	$0.69^{+0.03}_{-0.05}$	850	$13.1^{+0.2}_{-0.3}$
GW191204_110529	$47.2^{+9.2}_{-8.0}$	$19.8^{+3.6}_{-3.3}$	$27.3^{+11.0}_{-6.0}$	$19.3^{+5.6}_{-6.0}$	$0.05^{+0.26}_{-0.27}$	$1.8^{+1.7}_{-1.1}$	$0.34^{+0.25}_{-0.18}$	$45.0^{+8.6}_{-7.6}$	$0.71^{+0.12}_{-0.11}$	3700	$8.8^{+0.4}_{-0.6}$
GW191204_171526	$20.21^{+1.70}_{-0.96}$	$8.55^{+0.38}_{-0.27}$	$11.9^{+3.3}_{-1.8}$	$8.2^{+1.4}_{-1.6}$	$0.16^{+0.08}_{-0.05}$	$0.65^{+0.19}_{-0.25}$	$0.13^{+0.04}_{-0.05}$	$19.21^{+1.79}_{-0.95}$	$0.73^{+0.03}_{-0.03}$	350	$17.5^{+0.2}_{-0.2}$
GW191215_223052	$43.3^{+5.3}_{-4.3}$	$18.4^{+2.2}_{-1.7}$	$24.9^{+7.1}_{-4.1}$	$18.1^{+3.8}_{-4.1}$	$-0.04^{+0.17}_{-0.21}$	$1.93^{+0.89}_{-0.86}$	$0.35^{+0.13}_{-0.14}$	$41.4^{+5.1}_{-4.1}$	$0.68^{+0.07}_{-0.07}$	530	$11.2^{+0.3}_{-0.4}$
GW191216_213338	$19.81^{+2.69}_{-0.94}$	$8.33^{+0.22}_{-0.19}$	$12.1^{+4.6}_{-2.3}$	$7.7^{+1.6}_{-1.9}$	$0.11^{+0.13}_{-0.06}$	$0.34^{+0.12}_{-0.13}$	$0.07^{+0.02}_{-0.03}$	$18.87^{+2.80}_{-0.94}$	$0.70^{+0.03}_{-0.04}$	490	$18.6^{+0.2}_{-0.2}$
GW191219_163120	$32.3^{+2.2}_{-2.7}$	$4.32^{+0.12}_{-0.17}$	$31.1^{+2.2}_{-2.8}$	$1.17^{+0.07}_{-0.06}$	$0.00^{+0.07}_{-0.09}$	$0.55^{+0.25}_{-0.16}$	$0.11^{+0.05}_{-0.03}$	$32.2^{+2.2}_{-2.7}$	$0.14^{+0.06}_{-0.06}$	1500	$9.1^{+0.5}_{-0.8}$
GW191222_033537	79^{+16}_{-11}	$33.8^{+7.1}_{-5.0}$	$45.1^{+10.9}_{-8.0}$	$34.7^{+9.3}_{-10.5}$	$-0.04^{+0.20}_{-0.25}$	$3.0^{+1.7}_{-1.7}$	$0.51^{+0.23}_{-0.26}$	$75.5^{+15.3}_{-9.9}$	$0.67^{+0.08}_{-0.11}$	2000	$12.5^{+0.2}_{-0.3}$
GW191230_180458	86^{+19}_{-12}	$36.5^{+8.2}_{-5.6}$	$49.4^{+14.0}_{-9.6}$	37^{+11}_{-12}	$-0.05^{+0.26}_{-0.31}$	$4.3^{+2.1}_{-1.9}$	$0.69^{+0.26}_{-0.27}$	82^{+17}_{-11}	$0.68^{+0.11}_{-0.13}$	1100	$10.4^{+0.3}_{-0.4}$
GW200105_162426	$11.0^{+1.5}_{-1.4}$	$3.42^{+0.08}_{-0.08}$	$9.0^{+1.7}_{-1.7}$	$1.91^{+0.33}_{-0.24}$	$0.00^{+0.13}_{-0.18}$	$0.27^{+0.12}_{-0.11}$	$0.06^{+0.02}_{-0.02}$	$10.7^{+1.5}_{-1.4}$	$0.43^{+0.05}_{-0.02}$	7900	$13.7^{+0.2}_{-0.4}$
GW200112_155838	$63.9^{+5.7}_{-4.6}$	$27.4^{+2.6}_{-2.1}$	$35.6^{+6.7}_{-4.5}$	$28.3^{+4.4}_{-5.9}$	$0.06^{+0.15}_{-0.15}$	$1.25^{+0.43}_{-0.46}$	$0.24^{+0.07}_{-0.08}$	$60.8^{+5.3}_{-4.3}$	$0.71^{+0.06}_{-0.06}$	4300	$19.8^{+0.1}_{-0.2}$
GW200115_042309	$7.4^{+1.8}_{-1.7}$	$2.43^{+0.05}_{-0.07}$	$5.9^{+2.0}_{-2.5}$	$1.44^{+0.85}_{-0.29}$	$-0.15^{+0.24}_{-0.42}$	$0.29^{+0.15}_{-0.10}$	$0.06^{+0.03}_{-0.02}$	$7.2^{+1.8}_{-1.7}$	$0.42^{+0.09}_{-0.05}$	370	$11.3^{+0.3}_{-0.5}$
GW200128_022011	75^{+17}_{-12}	$32.0^{+7.5}_{-5.5}$	$42.2^{+11.6}_{-8.1}$	$32.6^{+9.5}_{-9.2}$	$0.12^{+0.24}_{-0.25}$	$3.4^{+2.1}_{-1.8}$	$0.56^{+0.28}_{-0.28}$	71^{+16}_{-11}	$0.74^{+0.10}_{-0.10}$	2600	$10.6^{+0.3}_{-0.4}$
GW200129_065458	$63.4^{+4.3}_{-3.6}$	$27.2^{+2.1}_{-2.3}$	$34.5^{+9.9}_{-3.2}$	$28.9^{+3.4}_{-9.3}$	$0.11^{+0.11}_{-0.16}$	$0.90^{+0.29}_{-0.38}$	$0.18^{+0.05}_{-0.07}$	$60.3^{+4.0}_{-3.3}$	$0.73^{+0.06}_{-0.05}$	130	$26.8^{+0.2}_{-0.2}$
GW200202_154313	$17.58^{+1.78}_{-0.67}$	$7.49^{+0.24}_{-0.20}$	$10.1^{+3.5}_{-1.4}$	$7.3^{+1.1}_{-1.7}$	$0.04^{+0.13}_{-0.06}$	$0.41^{+0.15}_{-0.16}$	$0.09^{+0.03}_{-0.03}$	$16.76^{+1.87}_{-0.66}$	$0.69^{+0.03}_{-0.04}$	170	$10.8^{+0.2}_{-0.4}$
GW200208_130117	$65.4^{+7.8}_{-6.8}$	$27.7^{+3.6}_{-3.1}$	$37.8^{+9.2}_{-6.2}$	$27.4^{+6.1}_{-7.4}$	$-0.07^{+0.22}_{-0.27}$	$2.23^{+1.00}_{-0.85}$	$0.40^{+0.15}_{-0.14}$	$62.5^{+7.3}_{-6.4}$	$0.66^{+0.09}_{-0.13}$	30	$10.8^{+0.3}_{-0.4}$
GW200208_222617	63^{+100}_{-25}	$19.6^{+10.7}_{-5.1}$	51^{+104}_{-30}	$12.3^{+9.0}_{-5.7}$	$0.45^{+0.43}_{-0.44}$	$4.1^{+4.4}_{-1.9}$	$0.66^{+0.54}_{-0.28}$	61^{+100}_{-25}	$0.83^{+0.14}_{-0.27}$	2000	$7.4^{+1.4}_{-1.2}$
GW200209_085452	$62.6^{+13.9}_{-9.4}$	$26.7^{+6.0}_{-4.2}$	$35.6^{+10.5}_{-6.8}$	$27.1^{+7.8}_{-7.8}$	$-0.12^{+0.24}_{-0.30}$	$3.4^{+1.9}_{-1.8}$	$0.57^{+0.25}_{-0.26}$	$59.9^{+13.1}_{-8.9}$	$0.66^{+0.10}_{-0.12}$	730	$9.6^{+0.4}_{-0.5}$
GW200210_092254	$27.0^{+7.1}_{-4.3}$	$6.56^{+0.38}_{-0.40}$	$24.1^{+7.5}_{-4.6}$	$2.83^{+0.47}_{-0.42}$	$0.02^{+0.22}_{-0.21}$	$0.94^{+0.43}_{-0.34}$	$0.19^{+0.08}_{-0.06}$	$26.7^{+7.2}_{-4.3}$	$0.34^{+0.13}_{-0.08}$	1800	$8.4^{+0.5}_{-0.7}$
GW200216_220804	81^{+20}_{-14}	$32.9^{+9.3}_{-8.5}$	51^{+22}_{-13}	30^{+14}_{-16}	$0.10^{+0.34}_{-0.36}$	$3.8^{+3.0}_{-2.0}$	$0.63^{+0.37}_{-0.29}$	78^{+19}_{-13}	$0.70^{+0.14}_{-0.24}$	2900	$8.1^{+0.4}_{-0.5}$
GW200219_094415	$65.0^{+12.6}_{-8.2}$	$27.6^{+5.6}_{-3.8}$	$37.5^{+10.1}_{-6.9}$	$27.9^{+7.4}_{-8.4}$	$-0.08^{+0.23}_{-0.29}$	$3.4^{+1.7}_{-1.5}$	$0.57^{+0.22}_{-0.22}$	$62.2^{+11.7}_{-7.8}$	$0.66^{+0.10}_{-0.13}$	700	$10.7^{+0.3}_{-0.5}$
GW200220_061928	148^{+55}_{-33}	62^{+23}_{-15}	87^{+40}_{-23}	61^{+26}_{-25}	$0.06^{+0.40}_{-0.38}$	$6.0^{+4.8}_{-3.1}$	$0.90^{+0.55}_{-0.40}$	141^{+51}_{-31}	$0.71^{+0.15}_{-0.17}$	3000	$7.2^{+0.4}_{-0.7}$
GW200220_124850	67^{+17}_{-12}	$28.2^{+7.3}_{-5.1}$	$38.9^{+14.1}_{-8.6}$	$27.9^{+9.2}_{-9.0}$	$-0.07^{+0.27}_{-0.33}$	$4.0^{+2.8}_{-2.2}$	$0.66^{+0.36}_{-0.31}$	64^{+16}_{-11}	$0.67^{+0.11}_{-0.14}$	3200	$8.5^{+0.3}_{-0.5}$
GW200224_222234	$72.2^{+7.2}_{-5.1}$	$31.1^{+3.2}_{-2.6}$	$40.0^{+6.9}_{-4.5}$	$32.5^{+5.0}_{-7.2}$	$0.10^{+0.15}_{-0.15}$	$1.71^{+0.49}_{-0.64}$	$0.32^{+0.08}_{-0.11}$	$68.6^{+6.6}_{-4.7}$	$0.73^{+0.07}_{-0.07}$	50	$20.0^{+0.2}_{-0.2}$
GW200225_060421	$33.5^{+3.6}_{-3.0}$	$14.2^{+1.5}_{-1.4}$	$19.3^{+5.0}_{-3.0}$	$14.0^{+2.8}_{-3.5}$	$-0.12^{+0.17}_{-0.28}$	$1.15^{+0.51}_{-0.53}$	$0.22^{+0.09}_{-0.10}$	$32.1^{+3.5}_{-2.8}$	$0.66^{+0.07}_{-0.13}$	370	$12.5^{+0.3}_{-0.4}$
GW200302_015811	$57.8^{+9.6}_{-6.9}$	$23.4^{+4.7}_{-3.0}$	$37.8^{+8.7}_{-8.5}$	$20.0^{+8.1}_{-5.7}$	$0.01^{+0.25}_{-0.26}$	$1.48^{+1.02}_{-0.70}$	$0.28^{+0.16}_{-0.12}$	$55.5^{+8.9}_{-6.6}$	$0.66^{+0.13}_{-0.15}$	6000	$10.8^{+0.3}_{-0.4}$
GW200306_093714	$43.9^{+11.8}_{-7.5}$	$17.5^{+3.5}_{-3.0}$	$28.3^{+17.1}_{-7.7}$	$14.8^{+6.5}_{-6.4}$	$0.32^{+0.28}_{-0.46}$	$2.1^{+1.7}_{-1.1}$	$0.38^{+0.24}_{-0.18}$	$41.7^{+12.3}_{-6.9}$	$0.78^{+0.11}_{-0.26}$	4600	$7.8^{+0.4}_{-0.6}$
GW200308_173609*	$50.6^{+10.9}_{-8.5}$	$19.0^{+4.8}_{-2.8}$	$36.4^{+11.2}_{-9.6}$	$13.8^{+7.2}_{-3.3}$	$0.65^{+0.17}_{-0.21}$	$5.4^{+2.7}_{-2.6}$	$0.83^{+0.32}_{-0.35}$	$47.4^{+11.1}_{-7.7}$	$0.91^{+0.03}_{-0.08}$	2000	$7.1^{+0.5}_{-0.5}$
GW200311_115853	$61.9^{+5.3}_{-4.2}$	$26.6^{+2.4}_{-2.0}$	$34.2^{+6.4}_{-3.8}$	$27.7^{+4.1}_{-5.9}$	$-0.02^{+0.16}_{-0.20}$	$1.17^{+0.28}_{-0.40}$	$0.23^{+0.05}_{-0.07}$	$59.0^{+4.8}_{-3.9}$	$0.69^{+0.07}_{-0.08}$	35	$17.8^{+0.2}_{-0.2}$
GW200316_215756	$21.2^{+7.2}_{-2.0}$	$8.75^{+0.62}_{-0.55}$	$13.1^{+10.2}_{-2.9}$	$7.8^{+1.9}_{-2.9}$	$0.13^{+0.27}_{-0.10}$	$1.12^{+0.47}_{-0.44}$	$0.22^{+0.08}_{-0.08}$	$20.2^{+7.4}_{-1.9}$	$0.70^{+0.04}_{-0.04}$	190	$10.3^{+0.4}_{-0.7}$
GW200322_091133*	55^{+37}_{-27}	$15.5^{+15.7}_{-3.7}$	34^{+48}_{-18}	$14.0^{+16.8}_{-8.7}$	$0.24^{+0.45}_{-0.51}$	$3.6^{+7.0}_{-2.0}$	$0.60^{+0.84}_{-0.30}$	53^{+38}_{-26}	$0.78^{+0.16}_{-0.17}$	6500	$6.0^{+1.7}_{-1.2}$

GWTC-3 (Abbott et al. 2021)

Masses in the Stellar Graveyard

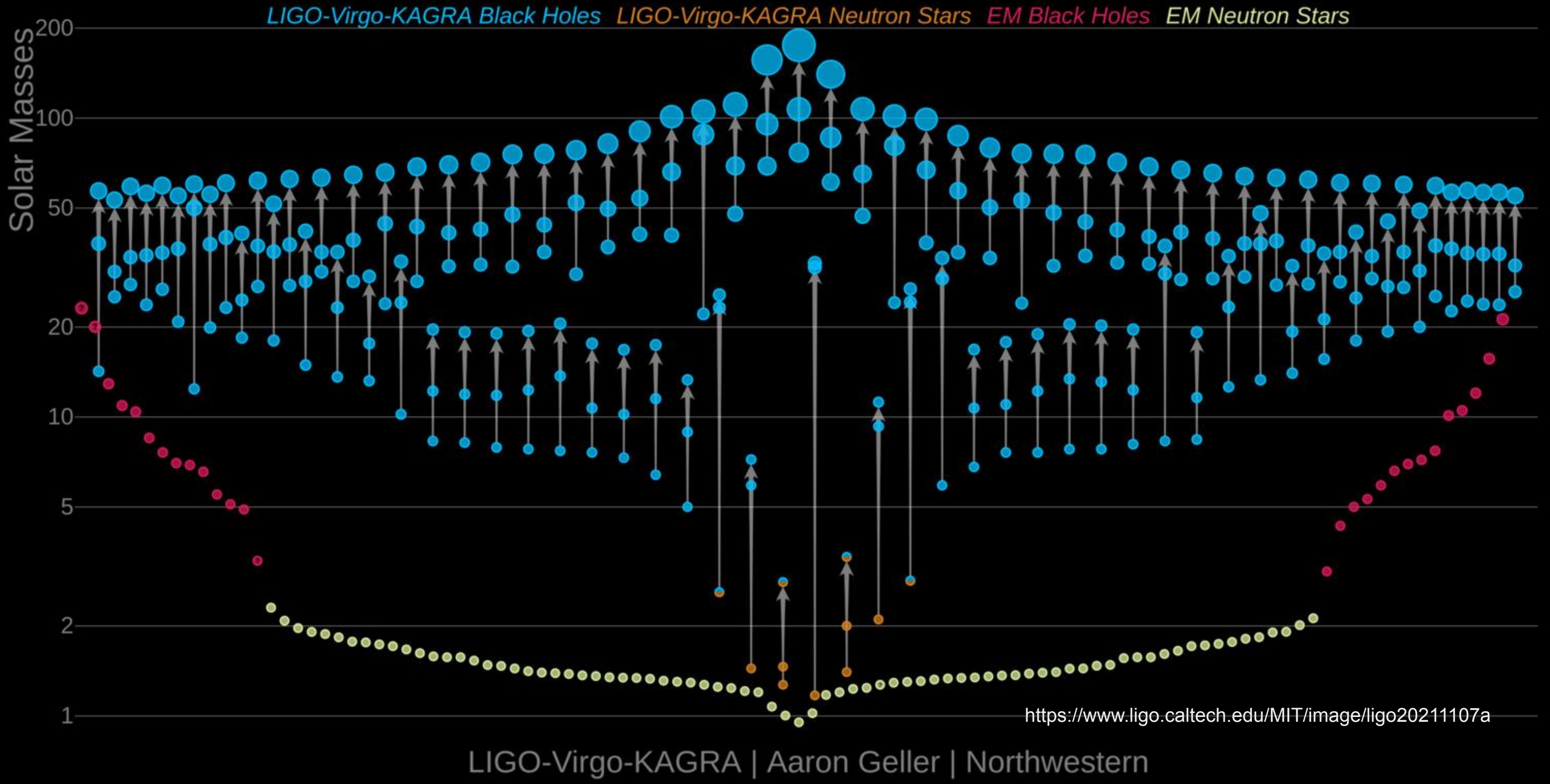

https://www.ligo.caltech.edu/MIT/image/ligo20211107a

Binary black holes (BBHs)

- More than 90% of GW sources ever detected
- Strong GW signal
- Detectable frequency for current interferometric GW detectors
- Predictable waveforms
- Coalescence
    - Inspiral - Merger - Ringdown

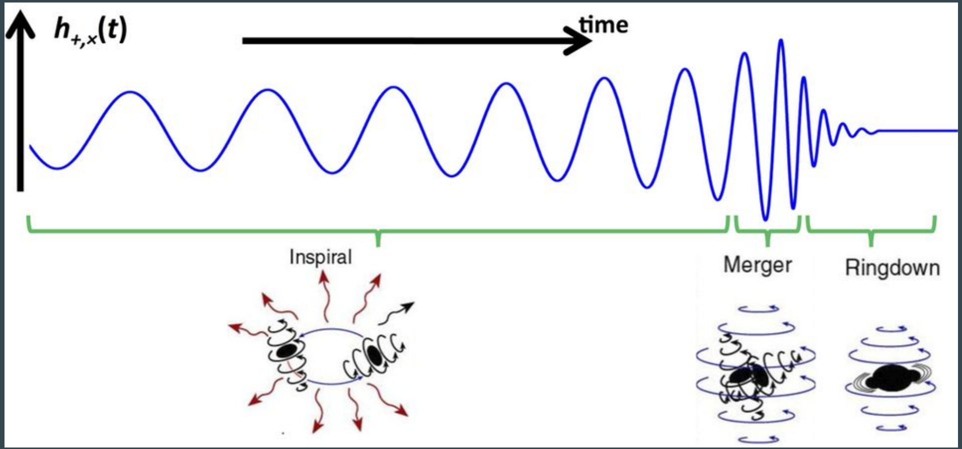

M. Favata/SXS/K. Thorne

Stellar Dynamics

BBH Formation

- Evolution of stellar binary

The Hubble Heritage Team (AURA/STScI/NASA) NASA Headquarters - Greatest Images of NASA (NASA-HQ-GRIN) - http://nix.larc.nasa.gov/info;jsessionid=1sl2so6lc9mab?id=GPN-2000-000933&orgid=12 http://imgsrc.hubblesite.org/hu/db/images/hs-1999-25-a-full_tif.tif

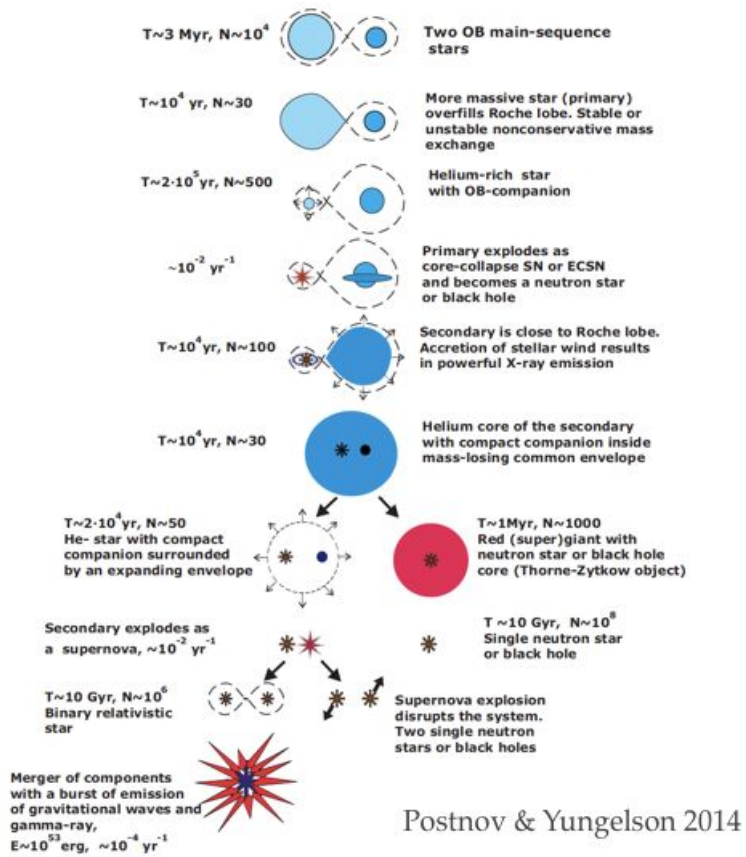

Figure 7: Evolutionary scenario for the formation of neutron stars or black holes in close binaries. T is the typical time scale of an evolutionary stage, N is the estimated number of objects in the given evolutionary stage.

BBH Formation

- Dynamical evolution of star cluster
  - Core collapse, Mass segregation
  - Binary formation, Binary heating
  - Hardening of binaries
  - Escape from cluster

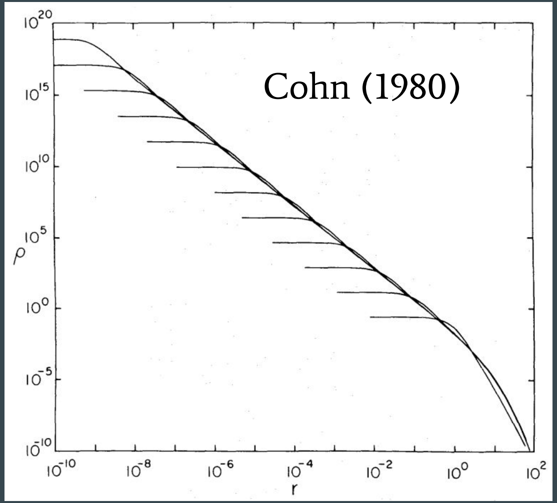

M80 (NGC 6093)

NASA, The Hubble Heritage Team, STScI, AURA - Great Images in NASA Description

Nuclear star cluster of Milky Way

Stefan Gillessen, Reinhard Genzel, Frank Eisenhauer - http://www.eso.org/public/outreach/press-rel/pr-2008/pr-46-08.html

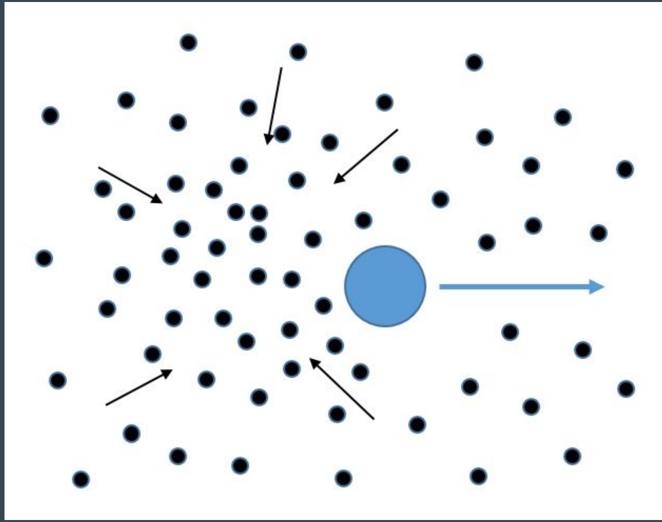

N-Body

N-body system

- Dynamical system of many particles
  - Astronomy
  - Molecular dynamics
  - Fluid dynamics
  - Ecology and evolutionary biology
  - Economics
  - Human activities
  - ...
- In Astronomy,
  - Planets, stars, galaxies, cosmology, ...

Two-body problem (in classical dynamics)

- System of two masses interacting through mutual gravitation
- Newton's law
- Analytical solution
  - Kepler orbit (point mass)
  - Circular, Elliptical, Parabolic, and Hyperbolic orbits

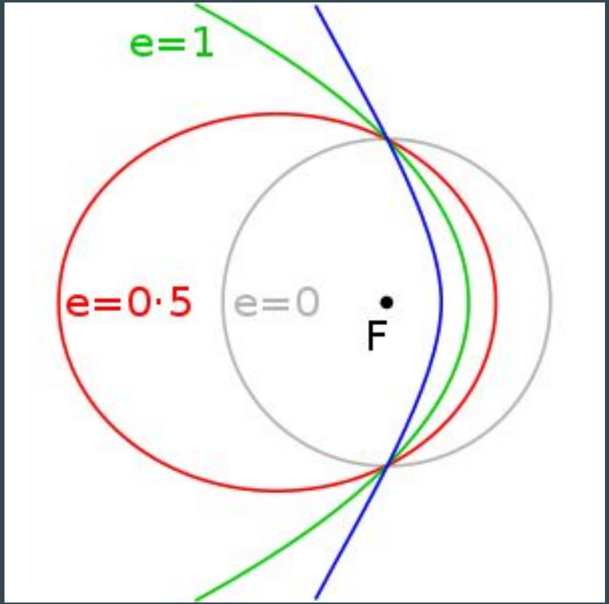

https://en.wikipedia.org/wiki/Kepler_orbit#/media/File:OrbitalEccentricityDemo.svg

Two-body problem (in classical dynamics)

- Elliptic orbit
  - Semi-major (a), semi-minor (b) axis

$$a = \frac{r_{max} + r_{min}}{2}, \quad b = \sqrt{r_{max} r_{min}}$$

  - Eccentricity

$$e = \sqrt{1 - \frac{b^2}{a^2}}$$

$$r_{min} = a(1 - e), \quad r_{max} = a(1 + e)$$

  - Orbital period

$$T = 2\pi \sqrt{\frac{a^3}{G(m_1 + m_2)}}$$

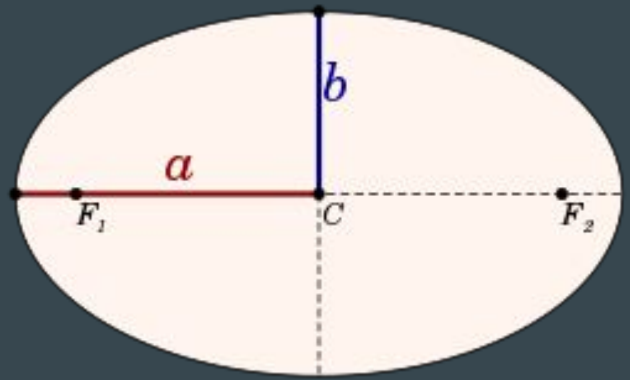

Two-body problem (in general relativity)

- Perihelion precession of Mercury’s orbit
- Orbital decay of Hulse-Taylor binary pulsar

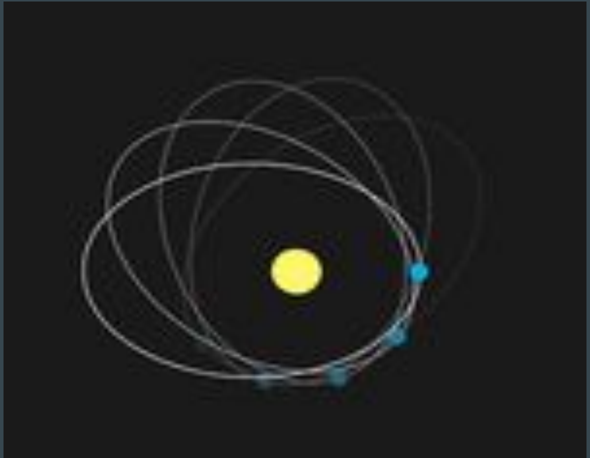

https://en.wikipedia.org/wiki/Tests_of_general_relativity#/media/File:Apsidendrehung.png

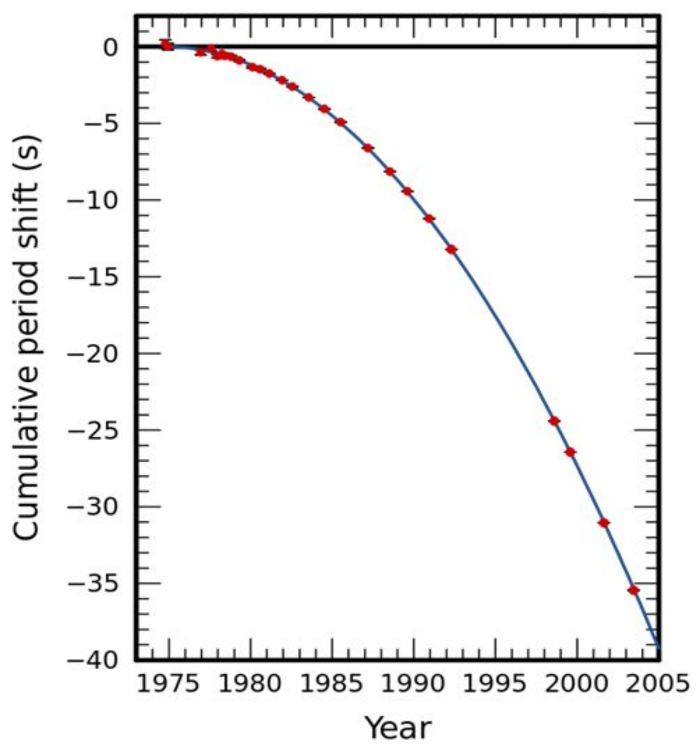

https://en.wikipedia.org/wiki/Hulse%E2%80%93Taylor_pulsar#/media/File:PSR_B1913+16_period_shift_graph.svg

Two-body problem (in general relativity)

- Einstein's theory of general relativity
- Considers gravitational effects due to the curvature of spacetime
- Test particle limit
  - Geodesic equation
  - Schwarzschild, Kerr metric
- Comparable mass
  - Approximation method for general relativity
    - Post-Newtonian, Post-Minkowskian, Effective-One-Body
  - Numerical relativity
- Spin effects

$$\frac{\mathrm{d}\boldsymbol{v}}{\mathrm{d}t} = -\frac{Gm}{r^2}\left[(1+\mathcal{A})\,\boldsymbol{n} + \mathcal{B}\,\boldsymbol{v}\right] + \mathcal{O}\left(\frac{1}{c^8}\right)$$

$$\begin{aligned}
\mathcal{A} = {} & \frac{1}{c^2}\left\{-\frac{3\dot{r}^2\nu}{2} + v^2 + 3\nu v^2 - \frac{Gm}{r}(4+2\nu)\right\} \\
& + \frac{1}{c^4}\left\{\frac{15\dot{r}^4\nu}{8} - \frac{45\dot{r}^4\nu^2}{8} - \frac{9\dot{r}^2\nu v^2}{2} + 6\dot{r}^2\nu^2 v^2 + 3\nu v^4 - 4\nu^2 v^4 \right. \\
& \qquad \left. + \frac{Gm}{r}\left(-2\dot{r}^2 - 25\dot{r}^2\nu - 2\dot{r}^2\nu^2 - \frac{13\nu v^2}{2} + 2\nu^2 v^2\right) + \frac{G^2m^2}{r^2}\left(9 + \frac{87\nu}{4}\right)\right\} \\
& + \frac{1}{c^5}\left\{-\frac{24\dot{r}\nu v^2}{5}\frac{Gm}{r} - \frac{136\dot{r}\nu}{15}\frac{G^2m^2}{r^2}\right\} \\
& + \frac{1}{c^6}\left\{-\frac{35\dot{r}^6\nu}{16} + \frac{175\dot{r}^6\nu^2}{16} - \frac{175\dot{r}^6\nu^3}{16} + \frac{15\dot{r}^4\nu v^2}{2} - \frac{135\dot{r}^4\nu^2 v^2}{4} + \frac{255\dot{r}^4\nu^3 v^2}{8} \right. \\
& \qquad - \frac{15\dot{r}^2\nu v^4}{2} + \frac{237\dot{r}^2\nu^2 v^4}{8} - \frac{45\dot{r}^2\nu^3 v^4}{2} + \frac{11\nu v^6}{4} - \frac{49\nu^2 v^6}{4} + 13\nu^3 v^6 \\
& \qquad + \frac{Gm}{r}\left(79\dot{r}^4\nu - \frac{69\dot{r}^4\nu^2}{2} - 30\dot{r}^4\nu^3 - 121\dot{r}^2\nu v^2 + 16\dot{r}^2\nu^2 v^2 + 20\dot{r}^2\nu^3 v^2 + \frac{75\nu v^4}{4} \right. \\
& \qquad\qquad \left. + 8\nu^2 v^4 - 10\nu^3 v^4\right) \\
& \qquad + \frac{G^2m^2}{r^2}\left(\dot{r}^2 + \frac{32573\dot{r}^2\nu}{168} + \frac{11\dot{r}^2\nu^2}{8} - 7\dot{r}^2\nu^3 + \frac{615\dot{r}^2\nu\pi^2}{64} - \frac{26987\nu v^2}{840} + \nu^3 v^2 \right. \\
& \qquad\qquad \left. - \frac{123\nu\pi^2 v^2}{64} - 110\dot{r}^2\nu\ln\left(\frac{r}{r'_0}\right) + 22\nu v^2\ln\left(\frac{r}{r'_0}\right)\right) \\
& \qquad \left. + \frac{G^3m^3}{r^3}\left(-16 - \frac{437\nu}{4} - \frac{71\nu^2}{2} + \frac{41\nu\pi^2}{16}\right)\right\} \\
& + \frac{1}{c^7}\left\{\frac{Gm}{r}\dot{r}\left(\frac{366}{35}\nu v^4 + 12\nu^2 v^4 - 114 v^2\nu\dot{r}^2 - 12\nu^2 v^2\dot{r}^2 + 112\nu\dot{r}^4\right) \right. \\
& \qquad + \frac{G^2m^2}{r^2}\dot{r}\left(\frac{692}{35}\nu v^2 - \frac{724}{15}v^2\nu^2 + \frac{294}{5}\nu\dot{r}^2 + \frac{376}{5}\nu^2\dot{r}^2\right) \\
& \qquad \left. + \frac{G^3m^3}{r^3}\dot{r}\left(\frac{3956}{35}\nu + \frac{184}{5}\nu^2\right)\right\},
\end{aligned}$$

$$\begin{aligned}
\mathcal{B} = {} & \frac{1}{c^2}\left\{-4\dot{r} + 2\dot{r}\nu\right\} \\
& + \frac{1}{c^4}\left\{\frac{9\dot{r}^3\nu}{2} + 3\dot{r}^3\nu^2 - \frac{15\dot{r}\nu v^2}{2} - 2\dot{r}\nu^2 v^2 + \frac{Gm}{r}\left(2\dot{r} + \frac{41\dot{r}\nu}{2} + 4\dot{r}\nu^2\right)\right\} \\
& + \frac{1}{c^5}\left\{\frac{8\nu v^2}{5}\frac{Gm}{r} + \frac{24\nu}{5}\frac{G^2m^2}{r^2}\right\} \\
& + \frac{1}{c^6}\left\{-\frac{45\dot{r}^5\nu}{8} + 15\dot{r}^5\nu^2 + \frac{15\dot{r}^5\nu^3}{4} + 12\dot{r}^3\nu v^2 - \frac{111\dot{r}^3\nu^2 v^2}{4} - 12\dot{r}^3\nu^3 v^2 - \frac{65\dot{r}\nu v^4}{8} \right. \\
& \qquad + 19\dot{r}\nu^2 v^4 + 6\dot{r}\nu^3 v^4 \\
& \qquad + \frac{Gm}{r}\left(\frac{329\dot{r}^3\nu}{6} + \frac{59\dot{r}^3\nu^2}{2} + 18\dot{r}^3\nu^3 - 15\dot{r}\nu v^2 - 27\dot{r}\nu^2 v^2 - 10\dot{r}\nu^3 v^2\right) \\
& \qquad \left. + \frac{G^2m^2}{r^2}\left(-4\dot{r} - \frac{18169\dot{r}\nu}{840} + 25\dot{r}\nu^2 + 8\dot{r}\nu^3 - \frac{123\dot{r}\nu\pi^2}{32} + 44\dot{r}\nu\ln\left(\frac{r}{r'_0}\right)\right)\right\} \\
& + \frac{1}{c^7}\left\{\frac{Gm}{r}\left(-\frac{626}{35}\nu v^4 - \frac{12}{5}\nu^2 v^4 + \frac{678}{5}\nu v^2\dot{r}^2 + \frac{12}{5}\nu^2 v^2\dot{r}^2 - 120\nu\dot{r}^4\right) \right. \\
& \qquad + \frac{G^2m^2}{r^2}\left(\frac{164}{21}\nu v^2 + \frac{148}{5}\nu^2 v^2 - \frac{82}{3}\nu\dot{r}^2 - \frac{848}{15}\nu^2\dot{r}^2\right) \\
& \qquad \left. + \frac{G^3m^3}{r^3}\left(-\frac{1060}{21}\nu - \frac{104}{5}\nu^2\right)\right\}.
\end{aligned}$$

Blanchet (2014)

Two-body problem (in general relativity)

- Dynamical capture (Gravitational-wave capture)
  - Unbound orbit to bound orbit by emitting GWs
  - Hyperbolic to elliptic orbit
  - Energy radiation > orbital energy

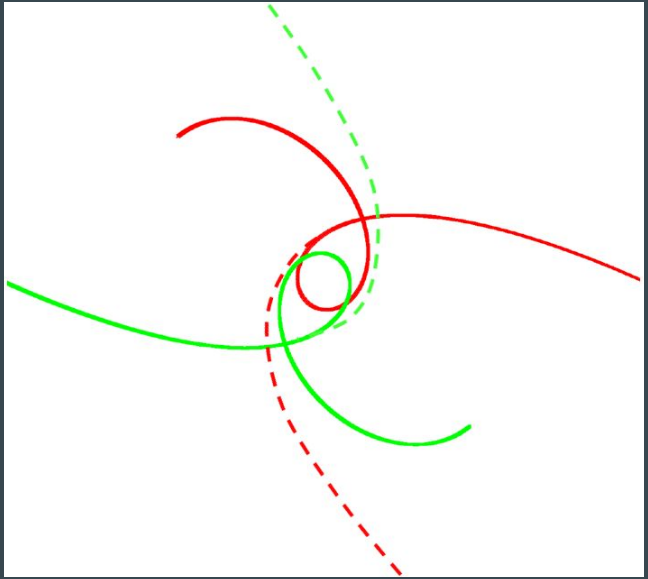

Two-body problem (in general relativity)

- GW radiation during the inspiral phase

$$h_+ = \frac{A}{r}(1+\cos^2 i)\cos(2\pi f t) f^{2/3}$$

$$h_\times = \frac{2A}{r}\cos i \sin(2\pi f t) f^{2/3}$$

$$A = 2\frac{G^{5/3}}{c^4}\pi^{2/3}M_c^{5/3}, \quad M_c \equiv \frac{(m_1 m_2)^{3/5}}{(m_1+m_2)^{1/5}}$$

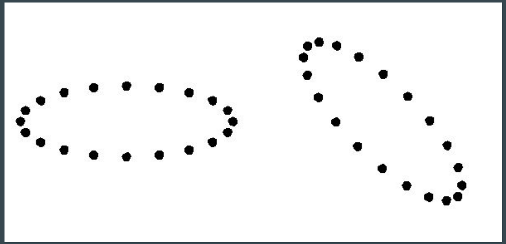

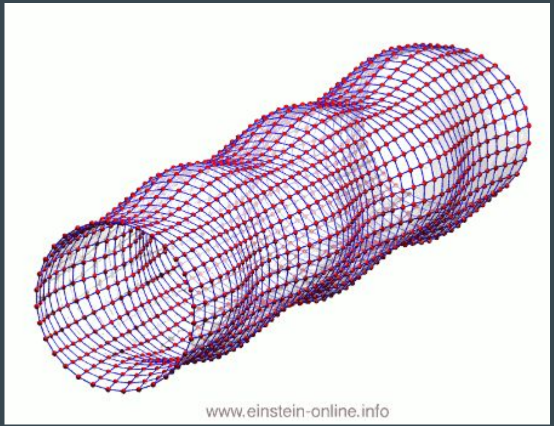

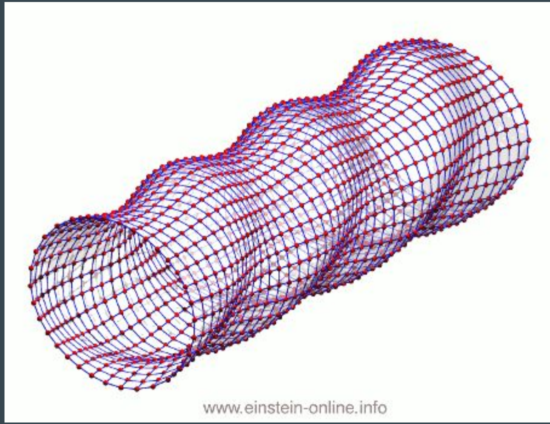

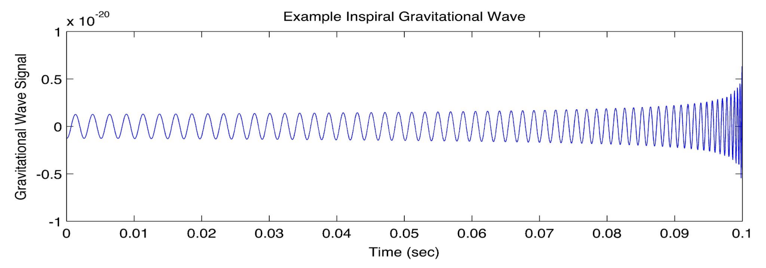

A. Stuver/LIGO, https://www.ligo.org/science/GW-Inspiral.php

Two-body problem (in general relativity)

- Circularization
  - Decrease of eccentricity
  - Why the quasi-circular orbit is considered primarily in the current GW detector

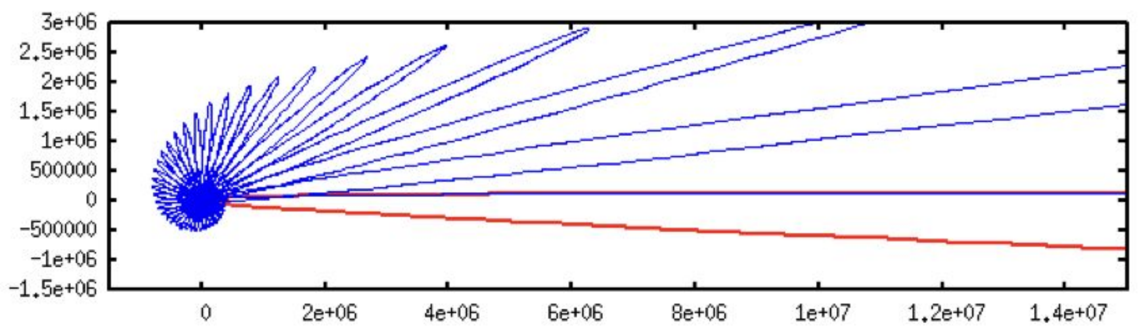

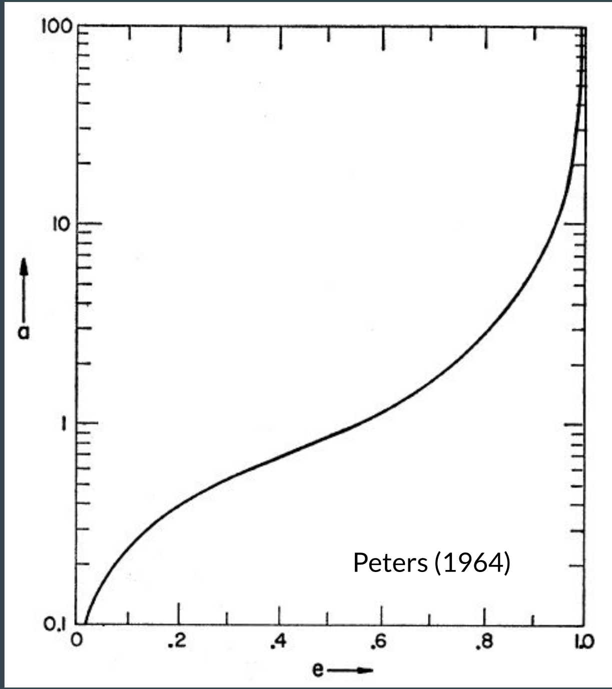

Peters (1964)

Three-body problem

- No general closed-form solution exists, generally chaotic.
- Restricted three-body problem
  - one negligible mass under two massive bodies
  - Lagrange points
- Special case solutions
  - Euler’s collinear solution, Figure-eight shape, ...
- Numerical methods are required in general.

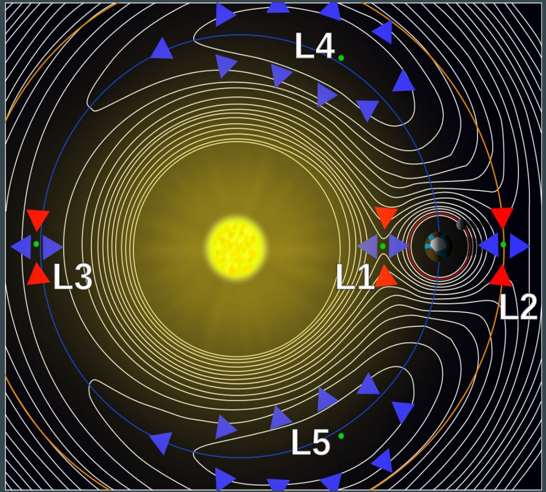

https://en.wikipedia.org/wiki/Lagrange_point#/media/File:Lagrange_points2.svg

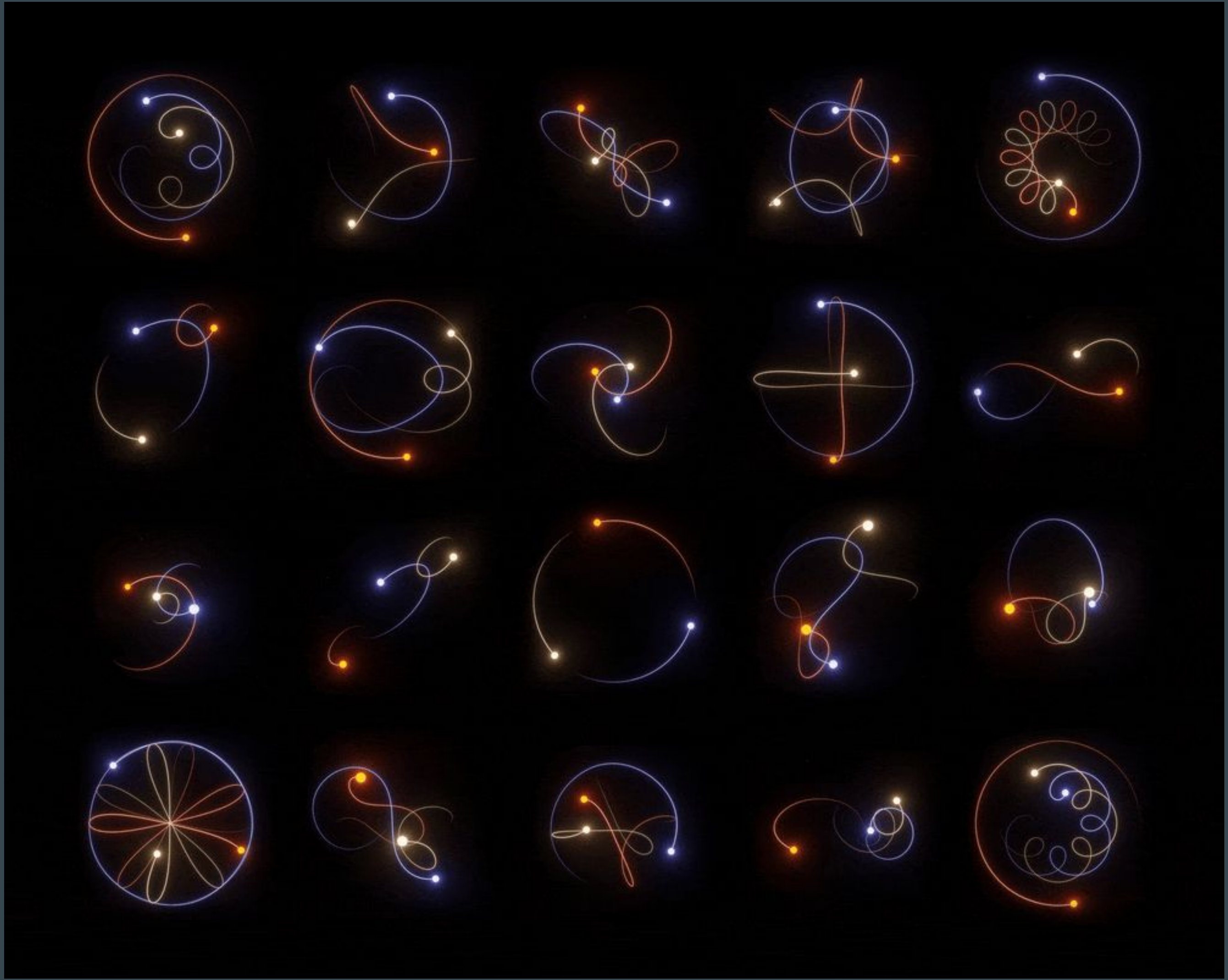

https://en.wikipedia.org/wiki/Three-body_problem#/media/File:5_4_800_36_downscaled.gif

Three-body problem

- Kozai-Lidov mechanism
  - Hierarchical triple system: Perturber is far from the other two masses
  - Oscillations in the eccentricity and inclination of the inner binary's orbit
  - Conservation of z-component angular momentum
  - Eccentric merger of binary black holes

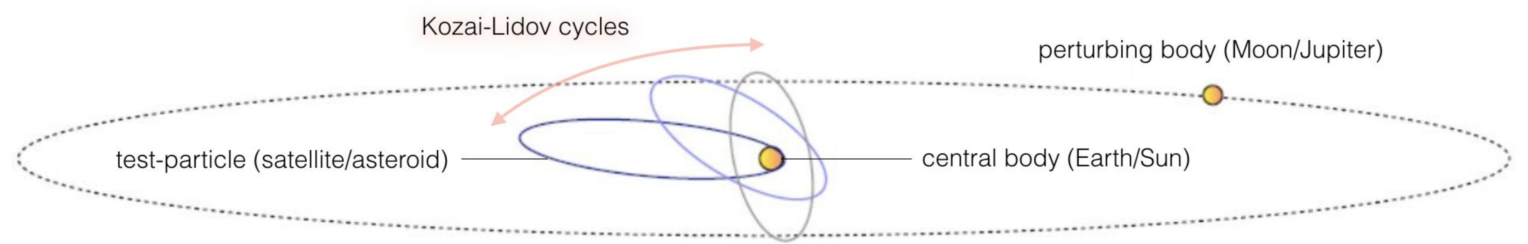

https://planetary.s3.amazonaws.com/web/assets/pictures/20180226_kozai-lidov-cycle.png

Three-body problem

- Three-body process
  - Binary formation through the interactions of three or more bodies

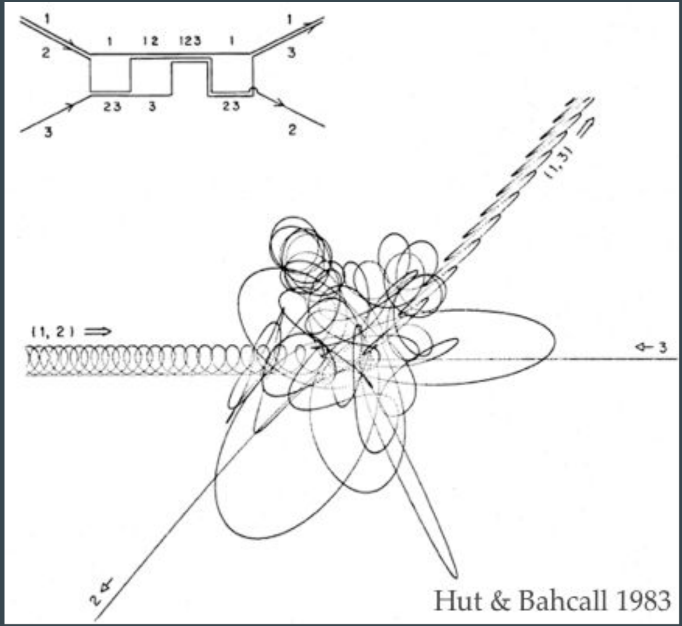

Three-body problem

- Binary-Single, Binary-Binary

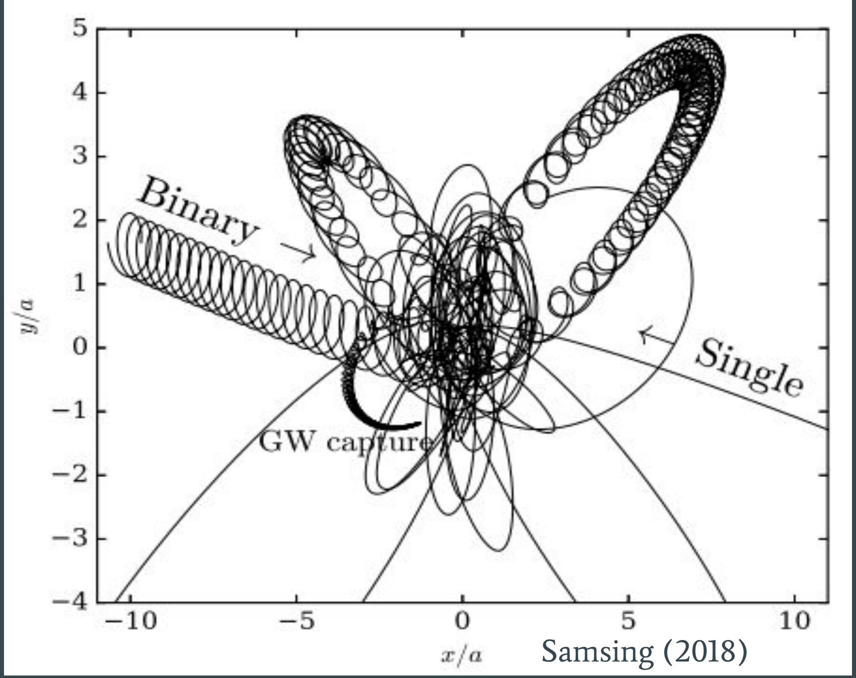

Samsing (2018)

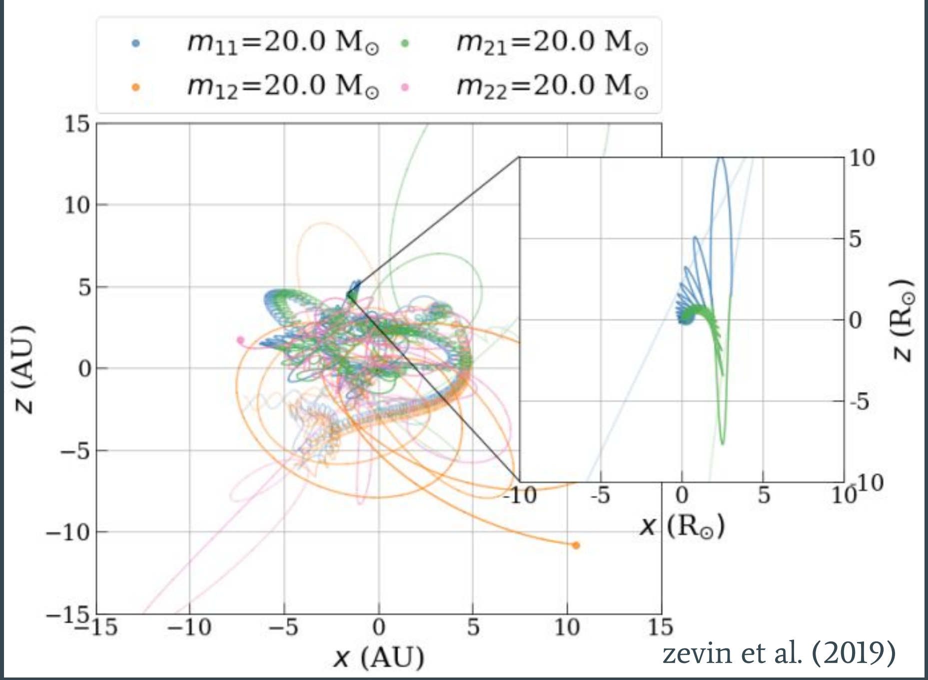

zevin et al. (2019)

N-body simulation

- N-body simulation
  - Numerical approach is generally required for N ≥ 3.
  - Direct N-body: $O(N^2)$ forces
  - Tree method (Barnes-Hut algorithm), Particle mesh, ...
  - Integration method
  - Time stepping
  - GPU

https://en.wikipedia.org/wiki/Barnes%E2%80%93Hut_simulation#/media/File:2D_Quad-Tree_partitioning_of_100_bodies.png

Summary

- Binary compact stars, which are the main sources of gravitational waves, can form in dense star clusters.
- N-body simulation is required for investigating stellar dynamics within clusters.
- In studies of binary compact stars, relativistic effects should be taken into account.